

Cite this: *Chem. Sci.*, 2024, **15**, 14721

All publication charges for this article have been paid for by the Royal Society of Chemistry

Received 29th June 2024
Accepted 12th August 2024

DOI: 10.1039/d4sc04292a

rsc.li/chemical-science

Introduction

In nature, a myriad of micro-scale machines endowed with motor functions, known as molecular motors, abound. These molecular motors fulfill diverse functions within organisms, playing integral roles in an array of life processes, ranging from DNA replication to cellular mitosis and beyond.^{1–4} Drawing inspiration from these natural wonders, chemists have undertaken the endeavor to create artificial molecular motors capable of controlled directional motion. These synthetic machines are designed to harness various external energy sources, such as photons,^{5–9} electricity,^{10–15} and chemical fuels,^{16–20} in pursuit of mimicking the remarkable capabilities observed in their biological counterparts.^{21,22}

Catenanes^{23,24} are a class of mechanically interlocked molecular architectures characterized by the topological entanglement of rings. Attributed to their dynamic behavior, which allows for reversible interconversion between different topological isomers in response to external stimuli, catenanes hold significant promise in the field of artificial molecular

machines (AMMs),^{25–27} particularly rotary motors. In 2003, Leigh and colleagues showcased the groundbreaking achievement of the synchronous unidirectional rotation in a [3]catenane rotary motor, completing a 360-degree revolution of two smaller rings along a larger circular track, marking the inception of catenane rotary motors.⁷ Subsequently, a [2]catenane rotary motor capable of selective rotation in either direction was developed.⁸ Building upon these advancements, in 2016, an autonomous [2]catenane rotary motor was introduced, operating through an innovative information ratchet mechanism.¹⁷ Additionally, Leigh's group reported a pioneering chemical-fueled [2]catenane rotary motor, driven by acid–base oscillations.¹⁸ More recently, a milestone was reached by Stoddart *et al.* with the development of an electricity-powered [3]catenane rotary motor, showcasing the unidirectional circumrotation of two CBPQT⁴⁺ rings around a 50-membered loop incorporated with a molecular pumping cassette.¹⁵ Despite these notable accomplishments, ongoing research efforts are focused on exploring catenane rotary motors with novel function mechanisms, aiming for heightened efficiency and precision in operation, as well as improved scalability to facilitate future applications.¹²

Recently, the benzimidazolium-based molecular pumping cassette demonstrates its capability in directionally collecting crown ether rings. Combining such a controlled molecular transportation with the clipping synthesis has led to precise radial catenanes (Fig. 1).²⁸ Encouragingly, we envision that the molecular pumping cassette could be further developed into a rotary motor operated *via* a flashing energy ratchet mechanism through alternate pumping and discharging. Herein, we present the molecular design, synthesis and precise operation of

^aSchool of Chemistry, Sun Yat-Sen University, Guangzhou, 510275, China. E-mail: zhukelong@mail.sysu.edu.cn

^bSchool of South China Academy of Advanced Optoelectronics, South China Normal University, Guangzhou, 510006, China

^cSchool of Chemistry and Chemical Engineering, Hainan University, Haikou, 570228, China

† Electronic supplementary information (ESI) available: Details of syntheses, ¹H NMR spectroscopy experiments and X-ray solutions for structures M–H (CCDC 2349579) and [1b–H₂–C24C6][BF₄] (CCDC 2349580). For ESI and crystallographic data in CIF or other electronic format see DOI: <https://doi.org/10.1039/d4sc04292a>



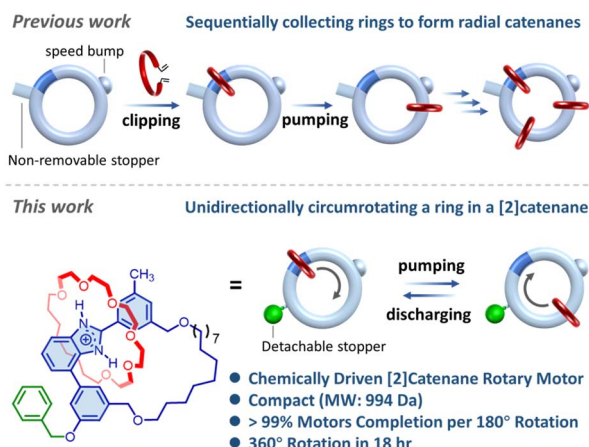


Fig. 1 Harnessing the benzimidazolium-based molecular pumping cassette to precisely construct radial catenanes (previous work) and to directionally operate a compact [2]catenane rotary motor via a flashing energy ratchet mechanism through alternate pumping and discharging (current work).

a compact [2]catenane rotary motor that is deemed the smallest (molecular weight ~ 994 Da) catenane rotary motor to date.

Results and discussion

As illustrated in Fig. 1, the [2]catenane rotary motor comprises a [24]crown-6 ether (**24C6**) wheel (red ring), a loop track molecule incorporating an L-shaped benzimidazolium pumping cassette (blue module within the large loop), and a detachable stopper (green sphere) facilitating controllable translocation of the **24C6** wheel upon chemical transformations. To power the motor, (i) the benzimidazolium is initially deprotonated to generate a thermo-dynamic driving force for shuttling the wheel towards the collecting moiety (phase A to B in Fig. 2); (ii) subsequent acidification progresses the motor to phase C, completing the pumping operation; (iii) cleavage of the stopper triggers a transition from phase C to D, relocating the wheel to

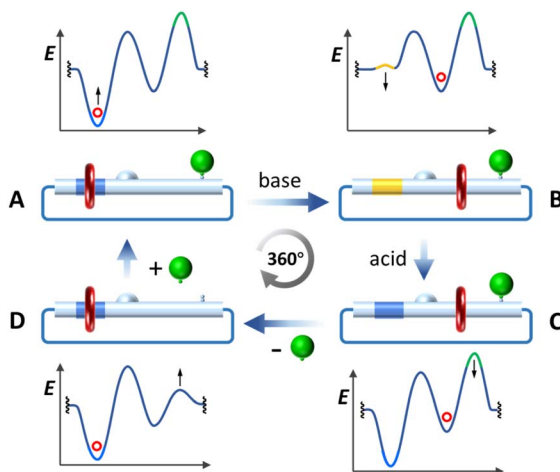


Fig. 2 Energy profiles for stages A–D through one 360-degree rotation of the [2]catenane rotary motor.

the benzimidazolium site; and (iv) re-stoppering finalizes the discharging operation (phase C to A) and resets the motor. Thus, by harnessing the net energy from acid–base and stoppering–detaching reactions, a unidirectional 360-degree rotation of the motor could be ultimately achieved through a flashing energy ratchet mechanism.⁸

Accordingly, to ensure successful unidirectional translocation of the wheel, it's imperative to determine if the **24C6** can thread through the L-shaped benzimidazoliums with or without a stoppering group.^{29,30} Consequently, $[1\mathbf{a}-\mathbf{H}_2]^+$ and $[1\mathbf{b}-\mathbf{H}_2]^+$ were initially synthesized and assessed for their complexation with **24C6** (see ESI† and Fig. 3a). No discernible association was observed between $[1\mathbf{a}-\mathbf{H}_2]^+$ and **24C6** under testing conditions (Fig. S1†), confirming that the 3-methoxy-5-methylphenyl moiety acts as a stopper for **24C6**. Conversely, ^1H NMR analysis of the mixture of $[1\mathbf{b}-\mathbf{H}_2]^+$ and **24C6** revealed a complexation with slow binding kinetics (Fig. 3b and S2†). Threading of **24C6** occurs upon heating at 65 °C indicating that the 3-hydroxyl-5-methylphenyl group is a slippage stopper for **24C6**. An association constant of $5.9 \times 10^3 \text{ M}^{-1}$ in CD_3NO_2 was determined for the [2]pseudorotaxane complex $[1\mathbf{b}-\mathbf{H}_2 \subset \mathbf{24C6}]^+$ (Fig. S3†), whose structure was unambiguously elucidated by X-ray crystal structure analysis (Fig. 3c and Table S3†). These results strongly affirm the ability of the L-shaped benzimidazolium featuring a 3-hydroxyl-5-methylphenyl moiety to

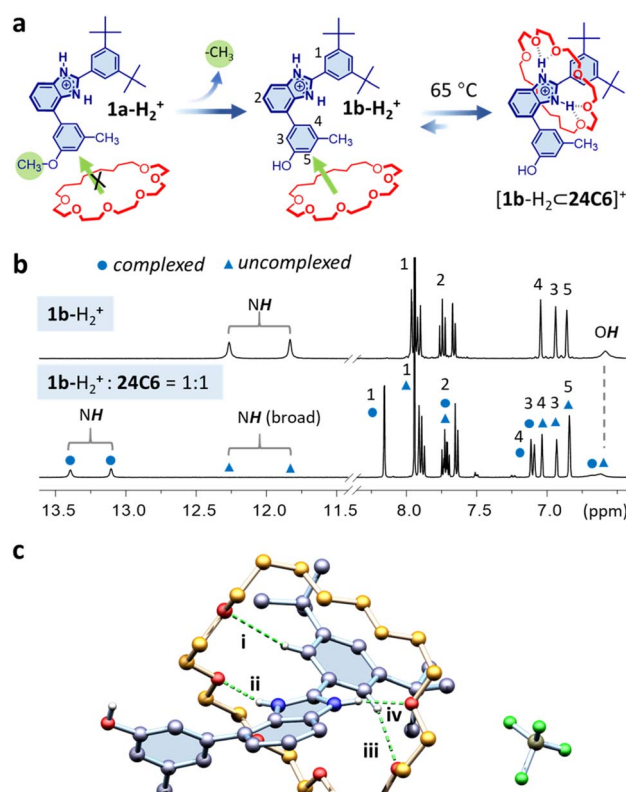


Fig. 3 (a) Schematic representation of threading **24C6** through L-shaped benzimidazoliums. (b) Partial ^1H NMR (400 MHz, 298 K, CD_3NO_2) spectra of an equimolar (2.0 mM) mixture of $[1\mathbf{b}-\mathbf{H}_2]^+$ and **24C6** before and after heating at 65 °C for 5 h. (c) Crystal structure of the complex $[1\mathbf{b}-\mathbf{H}_2 \subset \mathbf{24C6}]^+[\text{BF}_4^-]$. Hydrogen bonds: green dashed line.



translocate **24C6** in a directional manner when integrated into a [2]catenane rotary motor.

Subsequently, a loop molecule $[6\text{-H}_2]^+$, incorporating L-shaped benzimidazolium and a 14-membered aliphatic ring collecting moiety, was synthesized (see ESI† and Scheme 1). The hydroxyl [2]catenane $[\mathbf{M}\text{-H}_2]^+$ (where **M** denotes the motor) was then generated via Ru-catalyzed ring-closure metathesis (RCM), utilizing the bis-olefin precursor **24C6-pre** on $[6\text{-H}_2]^+$, followed by hydrogenation wherein de-benzylation occurred simultaneously. Acidification with HBF_4 finally afforded $[\mathbf{M}\text{-H}_2]^+$ (40% yield in 3 steps). The interlocked structure of $[\mathbf{M}\text{-H}_2]^+$ was confirmed by observing resonance signals for both cyclic components with a 1:1 integral ratio in ^1H NMR analysis (Fig. 4a and S33–S36†). The downfield chemical shifts for the NH protons (13.24 and 12.88 ppm corresponding to H_m and H_n , respectively) validate the presence of **24C6** at the benzimidazolium site primarily stabilized by $\text{N}-\text{H}\cdots\text{O}$ hydrogen bonds. This observation is consistent with the X-ray crystal structure of its neutral counterpart **M-H** resulting from deprotonation during crystallization (Fig. 5 and Table S4†).

The facile removal of the bulkier benzyl group under mild conditions, compared to a methyl group, has prompted us to explore its reinstallation onto $[\mathbf{M}\text{-H}_2]^+$ as the detachable stopper as originally designed (Fig. 1). However, prior to benzylation, it's crucial to assess the stability of $[\mathbf{M}\text{-H}_2]^+$ under basic conditions, as translocation of the **24C6** could occur when the benzimidazolium is deprotonated. Upon adding 10 equivalents of potassium carbonate to $[\mathbf{M}\text{-H}_2]^+$ in dimethyl sulfoxide, the formation of phenolate $[\mathbf{M}]^-$ was observed, while benzimidazolium was converted to benzimidazole, as verified by ^1H NMR analysis (see ESI and Fig. S4†). Furthermore, all the **24C6** wheels were confirmed to reside on the benzimidazole site, indicating no translocation occurs. Gratifyingly, almost identical resonance signals were noticed after heating at 90 °C for 20 h (Fig. S4d†), suggesting

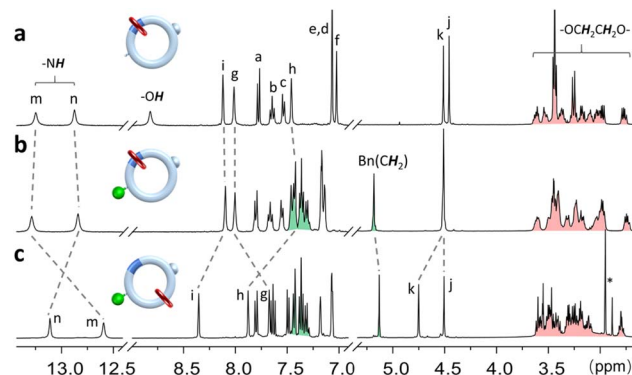
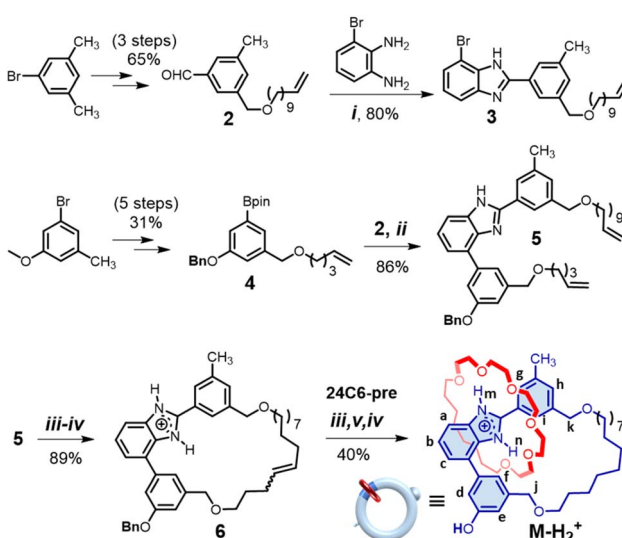


Fig. 4 Partial ^1H NMR (400 MHz, 298 K, CD_3CN) spectra of (a) $[\mathbf{M}\text{-H}_2]^+$, (b) $[\mathbf{I}\text{-BnM}\text{-H}_2]^+$, and (c) $[\mathbf{II}\text{-BnM}\text{-H}_2]^+$. Resonance peak assignment was referenced in Scheme 1. * impurity.

a significantly high energy barrier for threading the wheel in phenolate $[\mathbf{M}]^-$, which in turn could facilitate the reinstallation of the benzyl stopper. Consequently, implementing benzylation on $[\mathbf{M}\text{-H}_2]^+$ under the verified conditions efficiently afforded the [2]catenane rotary motor $[\mathbf{I}\text{-BnM}\text{-H}_2]^+$ as the sole product in an isolated yield of 82% (see ESI† and Fig. 4b). The complete disappearance of the ^1H NMR resonance signal for OH, coupled with the emergence of signals from the benzyl group, confirms the successful benzylation of $[\mathbf{M}\text{-H}_2]^+$. Furthermore, similar chemical shifts observed for NHs (13.29 ppm for H_m and 12.84 ppm for H_n) and ethylene protons, compared to $[\mathbf{M}\text{-H}_2]^+$, support the retention of the **24C6** on the benzimidazolium site.

The directional operation of motor $[\mathbf{I}\text{-BnM}\text{-H}_2]^+$ is demonstrated in Fig. 6, illustrating a complete 360° full rotation of the **24C6** wheel along the track loop, consisting of two half-circle rotations corresponding to the pumping and discharging steps, respectively. Initially, by harnessing the benzimidazolium pumping cassette, the **24C6** wheel undergoes a 180° clockwise rotation by converting $[\mathbf{I}\text{-BnM}\text{-H}_2]^+$ to its co-conformer $[\mathbf{II}\text{-BnM}\text{-H}_2]^+$ with the crown ether wheel positioned on the less-favored aliphatic moiety. Specifically, treatment of $[\mathbf{I}\text{-BnM}\text{-H}_2]^+$ with 5.0 equivalents of *t*-BuOK induces deprotonation, forming the metastable benzimidazolide species $[\mathbf{I}\text{-BnM}]^-$ (Fig. 7a). The



Scheme 1 Synthesis of the hydroxyl [2]catenane $[\mathbf{M}\text{-H}_2][\text{BF}_4]$. Conditions: (i) ZrCl_4 , CHCl_3 , 25 °C, 24 h; (ii) $\text{Pd}(\text{Ph}_3\text{P})_4$, 2 M Na_2CO_3 , THF , 80 °C, 4 h; (iii) Grubbs' catalyst, CH_2Cl_2 , 43 °C, 24 h; (iv) HBF_4 , 30 min; (v) H_2 , Pd/C , 25 °C, 4 h.

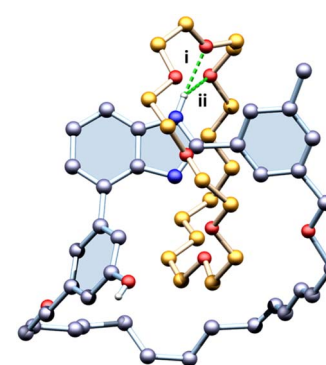


Fig. 5 Crystal structure of **M-H**. Hydrogen bonds are highlighted in the green dashed lines (i) and (ii). H atoms except OH and NH are omitted for clarity.



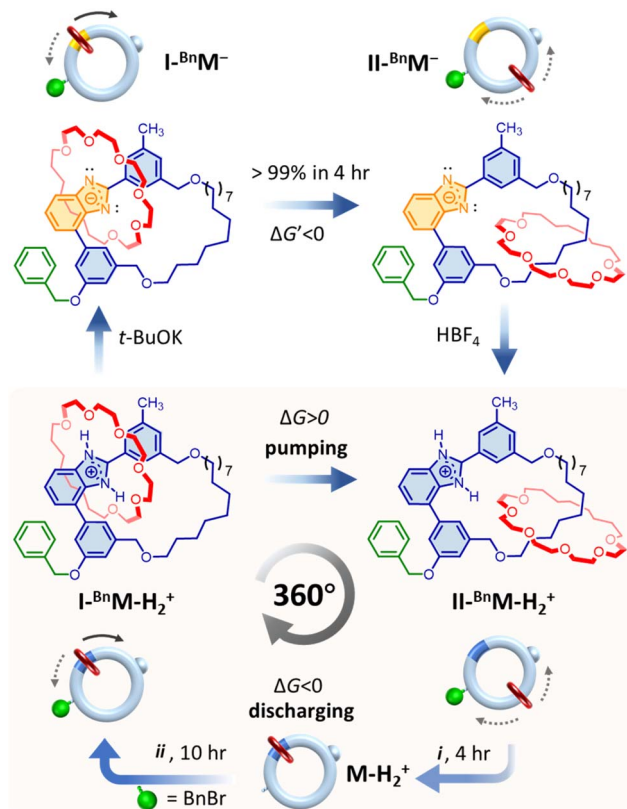


Fig. 6 Schematic representation of operating the [2]catenane rotary motor. Conditions: (i) H_2 , Pd/C , $25\text{ }^\circ\text{C}$; (ii) BnBr , K_2CO_3 , $90\text{ }^\circ\text{C}$.

electrostatic repulsion between the negative charged benzimidazolide and the electron-rich crown ether generates a thermodynamic driving force, leading to the sliding of the ring onto the alkyl moiety to yield its co-conformer $[\text{II}-\text{BnM}]^-$ (Fig. 6). A $\tau_{1/2}$ of 76 min associated with an energy barrier of 25.8 kcal mol $^{-1}$ was determined for such a translocation occurring at 338 K (Fig. S5, S6 and Tables S1, S2 \dagger). As revealed by ^1H NMR (Fig. 7c), approximately 80% of the 24C6 was translocated after heating at 338 K for 3 h, while almost full translocation (>99%) could be

achieved in 12 h (Fig. 7d) or in 4 hours by elevating the temperature to 373 K (Fig. S7 \dagger). The co-conformational product $[\text{II}-\text{BnM}-\text{H}_2]^+$ can be promptly generated by acidification with HBF_4 , providing a purified product with a 78% yield over two steps (see ESI \dagger). The translocation of 24C6 was confirmed by ^1H NMR comparison (Fig. 4c). Protons H_m and H_g exhibit evident upfield chemical shifting (-0.76 and -0.33 ppm, respectively), suggesting the absence of hydrogen bonding. Conversely, noticeable downfield chemical shifting is observed for H_n ($+0.27$ ppm), H_i ($+0.25$ ppm), H_h ($+0.41$ ppm), and H_k ($+0.25$ ppm), verifying the presence of 24C6 on the alkyl moiety with close proximity to the tolyl moiety. Additionally, 2D nuclear Overhauser enhancement spectroscopy (NOESY) (Fig. S44 \dagger) further supported the inferred structure of $[\text{II}-\text{BnM}-\text{H}_2]^+$, confirming the successful completion of the half-circle rotation. To power such a pumping process, a chemical energy input of 219.5 kcal mol $^{-1}$ could be estimated (see ESI \dagger).

To fulfill the 360° rotation of the motor, $[\text{II}-\text{BnM}-\text{H}_2]^+$ was then subjected to the discharging process, that is recovering $[\text{II}-\text{BnM}-\text{H}_2]^+$ to $[\text{I}-\text{BnM}-\text{H}_2]^+$ with the 24C6 wheel relocated to the benzimidazolium site. As mentioned earlier, removal of the stoppering benzyl group should generate a thermodynamic driving force favoring the benzimidazolium over the alkyl moiety for 24C6. Consequently, implementing palladium-catalyzed hydrogenation on $[\text{II}-\text{BnM}-\text{H}_2]^+$ (at 298 K, in 4 h) yielded the hydroxyl [2]catenane $[\text{M}-\text{H}_2]^+$ quantitatively, as evidenced by ^1H NMR (Fig. S8 \dagger). This implies that clock-wisely translocating the 24C6 wheel along the large loop is much faster than that observed for threading 24C6 onto $[\text{1b}-\text{H}_2]^+$ to form the [2]pseudorotaxane $[\text{1b}-\text{H}_2 \subset 24\text{C6}]^+$. Ultimately, repeating the benzylation of $[\text{M}-\text{H}_2]^+$ completes the discharging process and resets the motor to $[\text{I}-\text{BnM}-\text{H}_2]^+$, accomplishing the full circumvolution of the 24C6 wheel in the [2]catenane rotary motor. Correspondingly, an estimated chemical energy input of 195.3 kcal mol $^{-1}$ is required for achieving the second half-rotation (see ESI \dagger).

Conclusions

In summary, we present a compact and highly efficient [2]catenane rotary motor powered by chemical fuels. This motor accomplishes a full 360° unidirectional rotation through precisely controlled steps, employing a benzimidazolium-crown ether pumping cassette. The process involves distinct pumping and discharging phases: pumping drives a 180° rotation of the 24C6 wheel, while discharging resets the motor to its original state. Detailed experimental protocols confirm the motor's precision and efficiency, laying the foundation for further advances in molecular machines and nanotechnology.

Experimental

All reagents purchased from commercial suppliers were directly used without further purification unless otherwise noted. Solvents were either used as purchased or degassed and dried under a Vigor VSGS-5 Solvent Purification System. Detailed synthetic procedures are listed in the ESI (Schemes S1–S3 \dagger). The

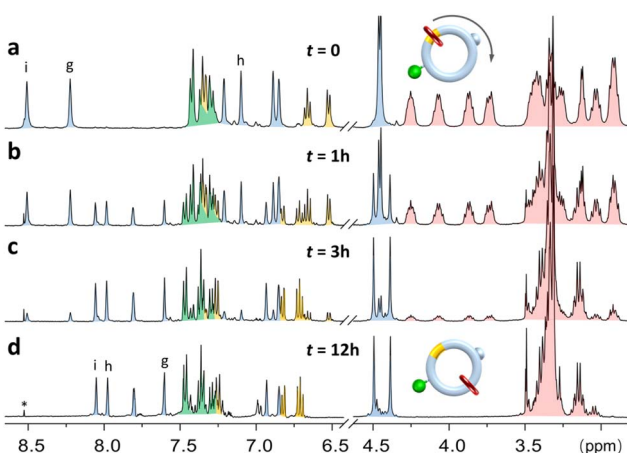


Fig. 7 Partial ^1H NMR (400 MHz, 298 K , $\text{DMSO}-d_6$) spectra of $[\text{I}-\text{BnM}]^-$ heated at 338 K for (a) 0 h ; (b) 1 h ; (c) 3 h ; and (d) 12 h * Impurity.



compounds were characterized by ^1H NMR, ^{13}C NMR, and 2D NMR spectroscopies (Fig. S9–S44†). NMR spectroscopy, host–guest complexation experiments and kinetics experiments (Fig. S2–S3 and S5†) were performed on a JEOL 400 YH instrument. X-ray diffraction analysis was performed either on a Rigaku SuperNova, Dual, AtlasS2 diffractometer using monochromatized Cu $\text{K}\alpha$ radiation or on a BRUKER D8 VENTURE PHOTON III diffractometer using Ga $\text{K}\alpha$ radiation. The crystal data are summarized in the ESI (Tables S3 and S4†).

Data availability

The data supporting this article have been included as part of the ESI.†

Author contributions

K. Z. supervised the project. A. L. performed all the synthetic experiments. A. L. collected and analyzed the NMR data with assistance from K. Z., Z. D., J. X., X. L. and Q. C. A. L. collected the SCXRD data. S. Z. and J. C. provided the SCXRD data analysis. K. Z. wrote the manuscript with input from A. L.

Conflicts of interest

There are no conflicts to declare.

Acknowledgements

We thank the National Natural Science Foundation of China (22171295), the Fundamental Research Funds for the Central Universities (23xkj006), the Starry Night Science Fund of Zhejiang University Shanghai Institute for Advanced Study (SN-ZJU-SIAS-006), and the Guangzhou Science and Technology Program (2024A04J6423) for financial support.

Notes and references

- 1 M. Schliwa and G. Woehlke, *Nature*, 2003, **422**(6933), 759–765.
- 2 C. Toyoshima and G. Inesi, *Annu. Rev. Biochem.*, 2004, **73**, 269–292.
- 3 C. von Ballmoos, G. M. Cook and P. Dimroth, *Annu. Rev. Biophys.*, 2008, **37**, 43–64.
- 4 *Molecular Machines in Biology: Workshop of the Cell*, ed. J. Frank, Cambridge University Press, 2011.
- 5 G. Ragazzon, M. Baroncini, S. Silvi, M. Venturi and A. Credi, *Nat. Nanotechnol.*, 2015, **10**(1), 70–75.
- 6 G. Ragazzon, M. Baroncini, S. Silvi, M. Venturi and A. Credi, *Beilstein J. Nanotechnol.*, 2015, **6**, 2096–2104.
- 7 D. A. Leigh, J. K. Y. Wong, F. Dehez and F. Zerbetto, *Nature*, 2003, **424**(6945), 174–179.
- 8 J. V. Hernandez, E. R. Kay and D. A. Leigh, *Science*, 2004, **306**(5701), 1532–1537.
- 9 H. Li, C. Cheng, P. R. McGonigal, A. C. Fahrenbach, M. Frasconi, W.-G. Liu, Z. Zhu, Y. Zhao, C. Ke, J. Lei, R. M. Young, S. M. Dyar, D. T. Co, Y.-W. Yang, Y. Y. Botros, W. A. Goddard III, M. R. Wasielewski, R. D. Astumian and J. F. Stoddart, *J. Am. Chem. Soc.*, 2013, **135**(49), 18609–18620.
- 10 C. Cheng, P. R. McGonigal, S. T. Schneebeli, H. Li, N. A. Vermeulen, C. Ke and J. F. Stoddart, *Nat. Nanotechnol.*, 2015, **10**(6), 547–553.
- 11 C. Pezzato, M. T. Nguyen, C. Cheng, D. J. Kim, M. T. Otley and J. F. Stoddart, *Tetrahedron*, 2017, **73**(33), 4849–4857.
- 12 Q.-H. Guo, Y. Qiu, X. Kuang, J. Liang, Y. Feng, L. Zhang, Y. Jiao, D. Shen, R. D. Astumian and J. F. Stoddart, *J. Am. Chem. Soc.*, 2020, **142**(34), 14443–14449.
- 13 Y. Qiu, B. Song, C. Pezzato, D. Shen, W. Liu, L. Zhang, Y. Feng, Q.-H. Guo, K. Cai, W. Li, H. Chen, M. T. Nguyen, Y. Shi, C. Cheng, R. D. Astumian, X. Li and J. F. Stoddart, *Science*, 2020, **368**(6496), 1247–1253.
- 14 J. S. W. Seale, B. Song, Y. Qiu and J. F. Stoddart, *J. Am. Chem. Soc.*, 2022, **144**(37), 16898–16904.
- 15 L. Zhang, Y. Qiu, W.-G. Liu, H. Chen, D. Shen, B. Song, K. Cai, H. Wu, Y. Jiao, Y. Feng, J. S. W. Seale, C. Pezzato, J. Tian, Y. Tan, X.-Y. Chen, Q.-H. Guo, C. L. Stern, D. Philp, R. D. Astumian, W. A. Goddard and J. F. Stoddart, *Nature*, 2023, **613**(7943), 280–286.
- 16 Z. Meng, J.-F. Xiang and C.-F. Chen, *J. Am. Chem. Soc.*, 2016, **138**(17), 5652–5658.
- 17 M. R. Wilson, J. Solà, A. Carbone, S. M. Goldup, N. Lebrasseur and D. A. Leigh, *Nature*, 2016, **534**(7606), 235–240.
- 18 S. Erbas-Cakmak, S. D. P. Fielden, U. Karaca, D. A. Leigh, C. T. McTernan, D. J. Tetlow and M. R. Wilson, *Science*, 2017, **358**(6361), 340–343.
- 19 S. Amano, S. D. P. Fielden and D. A. Leigh, *Nature*, 2021, **594**(7864), 529–534.
- 20 L. Binks, C. Tian, S. D. P. Fielden, I. J. Vitorica-Yrezabal and D. A. Leigh, *J. Am. Chem. Soc.*, 2022, **144**(34), 15838–15844.
- 21 Y. Feng, M. Ovalle, J. S. W. Seale, C. K. Lee, D. J. Kim, R. D. Astumian and J. F. Stoddart, *J. Am. Chem. Soc.*, 2021, **143**(15), 5569–5591.
- 22 R. D. Astumian, *Chem. Sci.*, 2017, **8**(2), 840–845.
- 23 J. P. Sauvage, *Angew. Chem. Int. Ed. Engl.*, 2017, **56**(37), 11080–11093; Q. Chen and K. Zhu, *Chem. Soc. Rev.*, 2024, **53**, 5677–5703.
- 24 V. K. Ahluwalia and R. Aggarwal, Catenanes, Rotaxanes and Knots, in *Alicyclic Chemistry*, ed. V. K. Ahluwalia and R. Aggarwal, Springer Nature, Cham, Switzerland, 2023, pp. 203–208.
- 25 S. Erbas-Cakmak, D. A. Leigh, C. T. McTernan and A. L. Nussbaumer, *Chem. Rev.*, 2015, **115**(18), 10081–10206.
- 26 S. Kassem, T. van Leeuwen, A. S. Lubbe, M. R. Wilson, B. L. Feringa and D. A. Leigh, *Chem. Soc. Rev.*, 2017, **46**(9), 2592–2621.
- 27 C. Pezzato, C. Cheng, J. F. Stoddart and R. D. Astumian, *Chem. Soc. Rev.*, 2017, **46**(18), 5491–5507; I. Aprahamian, *ACS Cent. Sci.*, 2020, **6**(3), 347–358.
- 28 A. Li, Z. Tan, Y. Hu, Z. Lu, J. Yuan, X. Li, J. Xie, J. Zhang and K. Zhu, *J. Am. Chem. Soc.*, 2022, **144**(5), 2085–2089.
- 29 N. Noujeim, K. Zhu, V. N. Vukotic and S. J. Loeb, *Org. Lett.*, 2012, **14**(10), 2484–2487.
- 30 H. Xu and K. Zhu, *Sci. Sin.: Chim.*, 2023, **53**(12), 2509–2522.

